

A Localization Method for First and Second Heart Sounds Based on Energy Detection and Interval Regulation

Se Dong Min* and Hangsik Shin[†]

Abstract – The present study suggests a localization method for the first (S_1) and the second (S_2) feature of heart sounds, based on an algorithm involving frequency filtering, energy detection, and interval regulation. Localization accuracy was evaluated by comparing the algorithm with the traditional Hilbert transform-based localization method. Results show that the sensitivity and the positive predictivity value of proposed method, respectively, were 97.27 % and 99.94 % in S_1 detection and 94.99 % and 100 % in S_2 detection.

Keywords: Energy detection, Heart sound, Hilbert transform, Interval regulation, Localization, Phonocardiogram (PCG)

1. Introduction

Auscultation, the action of listening to the internal sounds of the body using a stethoscope, is a simple and effective way to diagnosis of cardiac dysfunction and cardiovascular disease. Moreover, auscultation has been widely used for fundamental cardiac diagnoses because of its non-invasive and simple diagnostic characteristics. The major purpose of auscultation is listening to the heart sound caused by the closing of the heart valves. Heart sound contains many signals related to magnitude and frequency content, splitting, and the presence of additional systolic or diastolic murmur components. There are two dominant features of heart sounds: the first heart sound (S_1) and the second heart sound (S_2). S_1 reflects the closure of mitral and the tricuspid valves, and S_2 marks the closure of the aortic and pulmonary valves.

Heart sounds are usually investigated with S_1 and S_2 analysis. Because S_1 and S_2 occur at the onset of ventricular contraction and the end of ventricular systole, respectively, the left ventricular ejection time (LVET) and the pre-ejection period (PEP) have been estimated by heart sound analysis [1]. Moreover, the diagnosis of valve dysfunction and hemodynamic research are widely known applications of heart sound analysis. For example, cardiac valve disorder has been classified by a neural network classifier [2] and blood pressure has been estimated with pattern analysis [3] using heart sounds. Furthermore, the relationship between S_2 and aortic blood pressure has been shown [4]. Although heart sounds are a useful tool clinically, they are hard to analyze from the non-stationary characteristic. That is, making a cardiac disorder diagnosis based on heart sounds

is still a considerable challenge [5-12]. Thus, the accurate localization of S_1 and S_2 is an important issue for heart sound analysis and clinical applications.

Previous localization methods for heart sounds can be summarized as filtering, transform-based de-noising, and feature classification. In particular, wavelet de-noising has been researched to enable accurate heart sound localization [13-15]. There have been several approaches to S_1 and S_2 localization, such as spectral tracking [16], Shannon energy [17, 18], boundary modification method [19], time-delayed neural network [20], ECG-gated method [7], entropy based detection [21], homomorphic filtering [8], complexity based segmentation [22], hidden Markov model [23], and wavelet transform [24, 25]. Recently, wavelet de-noising and ECG-gated peak-peaking methods have been improved by an ensemble average method for more accurate localization [26]. Also, in 2012, S_1/S_2 heart sounds detection based on music beat tracking has been researched [27].

Most heart sound localization methods are based on the energy of the features. A problem with energy-based detection methods is the low amplitude of S_1 and S_2 components; they can easily be buried in background noise, murmurs, or lung sounds, and they are not reflected in the energy envelope of the heart sound [22]. Moreover, it has been shown that the amplitude of the heart sound waveform is changed by respiration [28]; the amplitude of the heart sound waveform is attenuated by inspiration. The ECG-gated localization method, a commonly used technique for the localization, is based on ECG features, such as the R-wave. ECG-gated localization provides relatively stable localization [26]. However, ECG should also be measured as a reference in the ECG-gated localization method. Moreover, for a variety of pathological conditions, there may be detection errors because of inconsistencies between the electrical and mechanical activities of the heart [29].

[†] Corresponding Author: Dept. of Biomedical Engineering, Chonnam National University, Korea. (hangsik.shin@jnu.ac.kr)

* Dept. of Medical IT Engineering, Soonchunhyang University, Korea. (sedongmin@sch.ac.kr)

Received: February 14, 2014; Accepted: May 12, 2015

The aim of the present study is the localization of S_1 and S_2 in heart sounds. In this study, features were discriminated from a phonocardiogram only. To improve localization performance, cascade integrator comb (CIC) filtering and an energy- and temporal-based localization method were developed. An experiment was performed in spontaneous and a 0.1 Hz or 0.25 Hz respiration-controlled environment to produce practical respiration effects and distortion. Statistical methods were used for a quantitative evaluation of the proposed algorithm.

2. Experimental Setup

2.1 Dataset

Eighteen young, healthy subjects (11 males, 7 females, mean age is 24.1, range 17-30 years old) participated. Prior to the experiment, the subjects were requested to provide information on their physical condition. None reported any taking medicine or signs of cardiovascular or respiratory disease. Each experiment was performed in a typical sports medicine laboratory at ambient room temperature, from 11 am to 6 pm. Drinking and smoking were prohibited during 24 hours and 2 hours before experiments, respectively. Anthropometric data, such as height and weight, were measured and are summarized in Table 1.

2.2 Devices and software

Heart sounds were recorded with a MP150 (Biopac Systems, inc., CA, USA), DA 100C acquisition module, and SS17L contact microphone. Heart sounds were measured on the chest surface between the 3rd and 4th ribs, and the ECG was measured on the chest surface with a Lead II configuration (Fig. 1). Acknowledge 3.9.1 (BIOPAC, USA) was used for real-time monitoring and data storage.

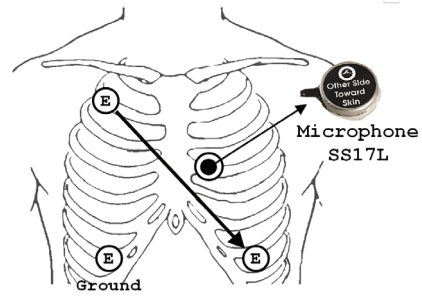


Fig. 1. Location of heart auscultation and ECG measurements

For signal conditioning, localization, and statistical analyses, MATLAB 2008b (Mathworks, Inc., Natick, MA, USA) was used and an HEM-907(Omron, Kyoto, Japan) was used for blood pressure measurements.

2.3 Experimental protocol

Heart sounds were measured, including spontaneous and controlled respiration effects. Respiration was controlled at 0.1 Hz (low rate) and 0.25 Hz (high rate) in a supine position using a metronome. In the sitting position, there was no respiration controlling. Experiments were carried out sequentially in the following order: spontaneous, 0.1 Hz controlled, and 0.25 Hz controlled respiration in the supine position, and spontaneous respiration in the sitting position. Subjects had a 2-min rest period between experiments. Data were sampled at a 1 kHz sampling rate for a 5-min period.

3. Signal Conditioning and Localization

3.1 Cascade integrator comb filter

CIC filtering has been used for biomedical signal conditioning and feature enhancement [29]. A CIC filter,

Table 1. Subject demographic data (^a Systolic Blood Pressure, ^b Diastolic blood pressure, ^c Heart rate (beats per minute))

Subject	Gender	Age	Height (cm)	Weight (kg)	BMI (kg/m ²)	SBP ^a (mmHg)	DBP ^b (mmHg)	HR (bpm) ^c
1	male	29	185	103	30.1	124 ± 5.7	70 ± 6.8	69.70 ± 7.23
2	male	30	172	81	27.6	139 ± 4.8	81 ± 4.9	82.80 ± 6.94
3	male	29	178	68	21.4	127 ± 13.7	73 ± 6.5	78.10 ± 2.22
4	male	28	175	78	25.3	122 ± 9.4	71 ± 2.2	61.95 ± 9.05
5	male	26	175	63	20.6	110 ± 3.5	66 ± 2.4	69.02 ± 3.26
6	female	26	161	57	22.2	100 ± 1.9	63 ± 2.0	57.04 ± 0.78
7	female	23	162	56	21.2	101 ± 3.7	67 ± 5.3	64.87 ± 4.07
8	female	21	161	60	23.1	107 ± 4.6	65 ± 3.4	79.73 ± 1.80
9	male	29	177	71	22.6	126 ± 10.7	72 ± 8.1	65.65 ± 3.29
10	male	24	171	68	23.1	135 ± 7.7	72 ± 7.4	68.82 ± 3.78
11	male	17	171	65	22.2	131 ± 8.4	67 ± 8.9	70.61 ± 2.97
12	female	22	159	47	18.5	103 ± 6.6	68 ± 4.7	78.98 ± 1.07
13	male	25	174	77	25.7	119 ± 9.3	72 ± 5.7	69.21 ± 1.74
14	female	22	163	55	20.5	107 ± 3.1	74 ± 5.6	80.14 ± 6.39
15	male	18	175	83	26.9	134 ± 9.1	75 ± 6.8	63.70 ± 5.16
16	male	23	172	71	24.2	140 ± 9.1	77 ± 12.5	56.46 ± 4.22
17	female	19	164	63	23.6	110 ± 2.9	69 ± 5.1	57.60 ± 5.30
18	female	21	160	60	23.6	120 ± 4.5	75 ± 5.7	61.49 ± 3.67

which is a linear-phase filter, was implemented for signal conditioning of the heart sounds. Linear phase-filtering, which prevents phase and timing distortion, is important because the heart sound has non-stationary characteristic. A CIC filter is composed of a high-pass and a low-pass filter and its transfer function is described in (1) and (2). N_{hpf} , N_{lpf} , and M indicate the high-pass filter order, low-pass filter order, and number of cascaded stages, respectively; their values were 16, 8, and 2, respectively, in the filter design. N_{hpf} , N_{lpf} , and M had a 43.2 Hz center frequency and pass-band between 26.6 Hz and 63 Hz (3 dB point). The frequency characteristics of the CIC filter are presented in Fig. 2(a).

$$H_{hpf}(z) = z^{-D} \cdot \left(\frac{1}{N_{hpf}} \cdot \frac{1 - z^{-N_{hpf}}}{1 - z^{-1}} \right)^M, \quad (1)$$

$$D = \frac{N_{hpf} - 1}{2} \cdot M$$

$$H_{lpf}(z) = \left(\frac{1}{N_{lpf}} \cdot \frac{1 - z^{-N_{lpf}}}{1 - z^{-1}} \right)^M \quad (2)$$

3.2 Moving average filter

A general heart sound is described with a high-frequency signal. However, specific features, such as S_1 and S_2 , are decided by the value of the envelope. From the natural

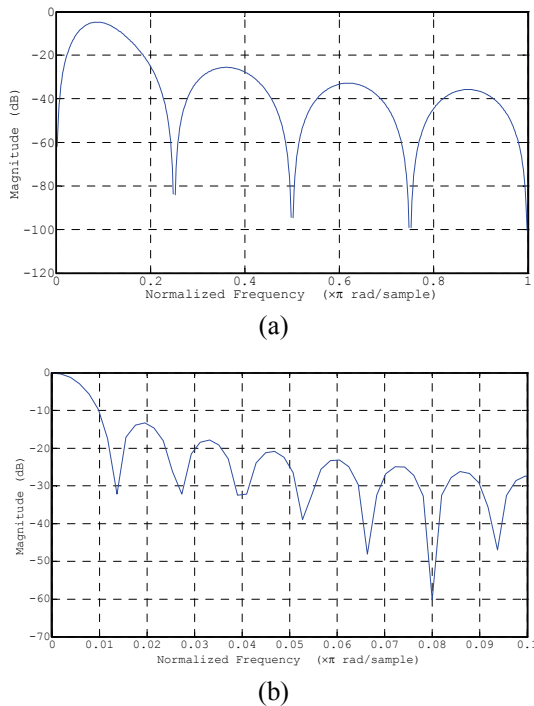


Fig. 2. Frequency characteristic of filters: (a) Cascade integrator comb filter. The center frequency is 43.2 Hz and the pass-band is 26.6 to 63 Hz; (b) Moving average filter (cut-off frequency is ~ 3 Hz)

characteristics of heart sounds, the envelope detected by the Hilbert transform contains many tiny fluctuations that could have an effect on specific feature extraction. These fluctuations are also regarded as high frequency noise in feature extraction; thus, a moving-average filter (MAF) was used for envelope smoothing as a kind of low-pass filter. The frequency response of MAF is shown in (3). L is the MAF length and it was of 0.15 s duration (cut-off frequency is ~ 3 Hz). Fig. 2(b) shows the frequency characteristics of MAF.

$$H_{MAF}(z) = \frac{1}{L} \cdot \frac{1 - z^{-L}}{1 - z^{-1}} \quad (3)$$

3.3 Hilbert transform

The Hilbert transform is proper for time-varying signal analysis, used frequently for envelope detection with heart sounds [31]. The analytic function of $z[n]$ contains a real-value function $x[n]$ and a complex value function $\tilde{x}[n]$, which is the Hilbert transform pair of $x[n]$. The analytical signal and envelope detection equations are described in (4) and (5), respectively.

$$z[n] = x[n] + j\tilde{x}[n] \quad (4)$$

$$Envelope[n] = \sqrt{x^2[n] + \tilde{x}^2[n]} \quad (5)$$

3.4 S_1 and S_2 Localization

The heart sound signal is processed sequentially, with CIC filtering, the Hilbert transformation, and moving-average filtering. Then, the S_1 and S_2 peaks are detected from the filtered envelope of the heart sound. S_1 peaks were detected by a zero-crossing method, based on signal derivation. For S_2 localization, an energy based detection method was used within the S_1 intervals. The S_1 -gated window was determined from the $(n-1)^{th}$ position of S_1 ($PS1_{n-1}$) to the n^{th} position of S_1 ($PS1_n$). A 0.2-s refractory period was also defined to reduce misdetection for the former and latter S_1 location. Thus, the scanning window

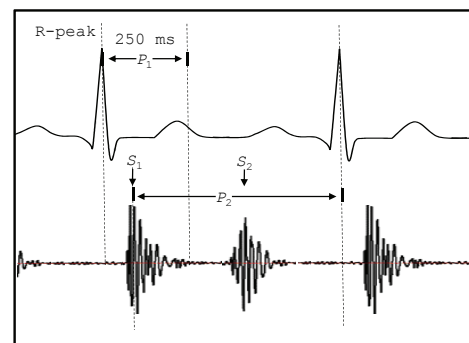


Fig. 3. Localization method of the reference S_1 and S_2 positions

had a range between $PS1_{n-1} + 0.2$ and $PS1_n - 0.2$. Within the scanning window, S_2 was localized by taking the maximum value of the energy waveform of the heart sound.

The reference peak position was detected by an ECG-gated detection method and the Hilbert transformation. The S_1 location was decided within a 250 ms detection window (P1) following the R peak of the ECG waveform. The S_2 location was detected by the maximum energy within the specified range (P_2). P_2 starts from the S_1 location to the next R peak of the ECG. Each detected S_1 and S_2 was corrected manually (Fig. 3).

3.5 Peak correction

The envelope of the heart sound has two distinguishable peaks, at S_1 and S_2 . In using time difference-based classification method, the detection of both S_1 and S_2 should precede S_1 and S_2 classification. The detected peaks are typically located at the S_1 and S_2 positions. However, redundant peaks or missed peaks may still remain. In the pre-processing stage of S_1 localization, mis-detected peak correction is directly related to detection accuracy. The proposed localization method is based on time difference characteristics between S_1 and S_2 . Because the S_2 - S_1 interval is generally longer than the S_1 - S_2 interval, the difference in peak time interval (PTI) can be described with an up-and-down curve. If we assume that every peak was detected correctly, then the PTI curve should be repeated with a regular up-and-down pattern. However, a PTI curve could show an irregular trend from missed or redundant peaks. In the missed peak case, PTI becomes higher than the normal upper limit (6) and redundant peaks causes a lower PTI value than the other lower peaks (7). To remove these irregularities, a peak correction method was used. Peak correction was carried out with two processes: False Positive Peak correction (FPPC) and False Negative Peak correction (FNPC). FPP correction modifies PTI values using (8); a redundant peak time interval at the nth PTI, PTI_n , is removed by comparison between the former and the latter PTI value. In the FNP correction, in contrast, a new PTI is added using (9). The estimated S_1 and S_2 intervals are decided by average values of 50% higher or lower.

$$PTI_n > \text{mean}(PTI) + 2.5\text{std}(PTI) \quad (6)$$

$$PTI_n < \text{mean}(PTI) - \text{std}(PTI) \quad (7)$$

$$\begin{cases} PTI_{n-1} = PTI_{n-1} + PTI_n, & PTI_{n-1} < PTI_{n+1} \\ PTI_{n+1} = PTI_{n+1} + PTI_n, & PTI_{n-1} > PTI_{n+1} \end{cases} \quad (8)$$

$$\begin{cases} PTI_{n+1} = PTI_{n+1} - EI_{s1}, & PTI_{n-1} < PTI_{n+1} \\ PTI_{n+1} = PTI_{n+1} - EI_{s2}, & PTI_{n-1} > PTI_{n+1} \end{cases} \quad (9)$$

Moreover, both S_1 and S_2 should be detected after the signal conditioning procedures and classified with PTI analysis for S_1 localization. Fig. 4 shows the PTI analysis

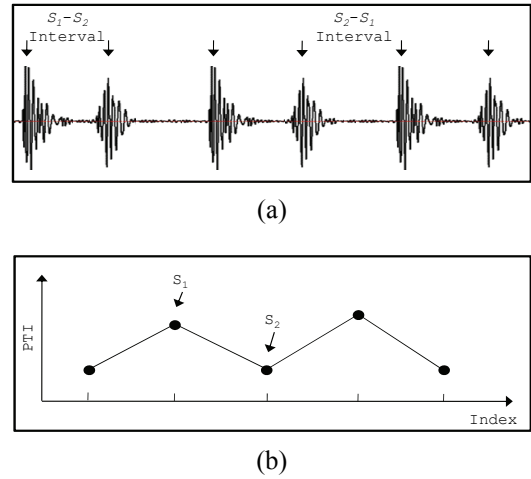


Fig. 4. Peak time interval (PTI) analysis and S1 localization: (a) Detected peaks and intervals between S_1 and S_2 ; (b) PTI and S_1 localization. S_1 is located at the up-to-down breakpoint.

procedure. PTI can be represented with an up-and-down plot in the general case, and the up-to-down breakpoint indicates the S_1 location.

3.6 Replace, add, and delete algorithm

As noted previously, a representative detection problem can be summarized with FPP and FNP. In S_1 classification, a similar problem occurs. Typically, FNP means missed peaks or confusing S_1 and S_2 . Moreover, FPP means that there are redundant peaks around the actual S_1 location. To improve this detection problem, a replace, add, and delete (RAD) algorithm is proposed.

Replace, add, and delete procedures are defined by PTI range. In the replace procedure, when S_2 is detected as a substitute of S_1 , PTI is between $Limit_{h1}$ and $Limit_{h2}$ ($Limit_{h1} < PTI < Limit_{h2}$). If PTI is longer than the replace interval ($Limit_{h2} < PTI$), it is regarded as an add procedure. The delete procedure is invoked when PTI is shorter than $Limit_{l1}$ ($Limit_{l1} > PTI$). Classification criteria, $Limit_{h1}$, $Limit_{h2}$, and $Limit_{l1}$, are determined using (10), (11) and (12), respectively, with empirical constant, and they are adaptively changed by the previous S_1 interval.

$$\begin{cases} Limit_{h1} = 1.2MBR_{TOTAL}, & \text{if previous peaks are not exist.} \\ Limit_{h1} = 1.4MBR_{prev} \end{cases} \quad (10)$$

$$\begin{cases} Limit_{h2} = 1.8MBR_{TOTAL}, & \text{if previous peaks are not exist.} \\ Limit_{h2} = 1.8MBR_{prev} \end{cases} \quad (11)$$

$$\begin{cases} Limit_{l1} = 0.4MBR_{TOTAL}, & \text{if previous peaks are not exist.} \\ Limit_{l1} = 0.5MBR_{prev} \end{cases} \quad (12)$$

Fig. 5 shows three detection problems and correction methods such as ‘Replace’, ‘Add’ and ‘Delete’ algorithm.

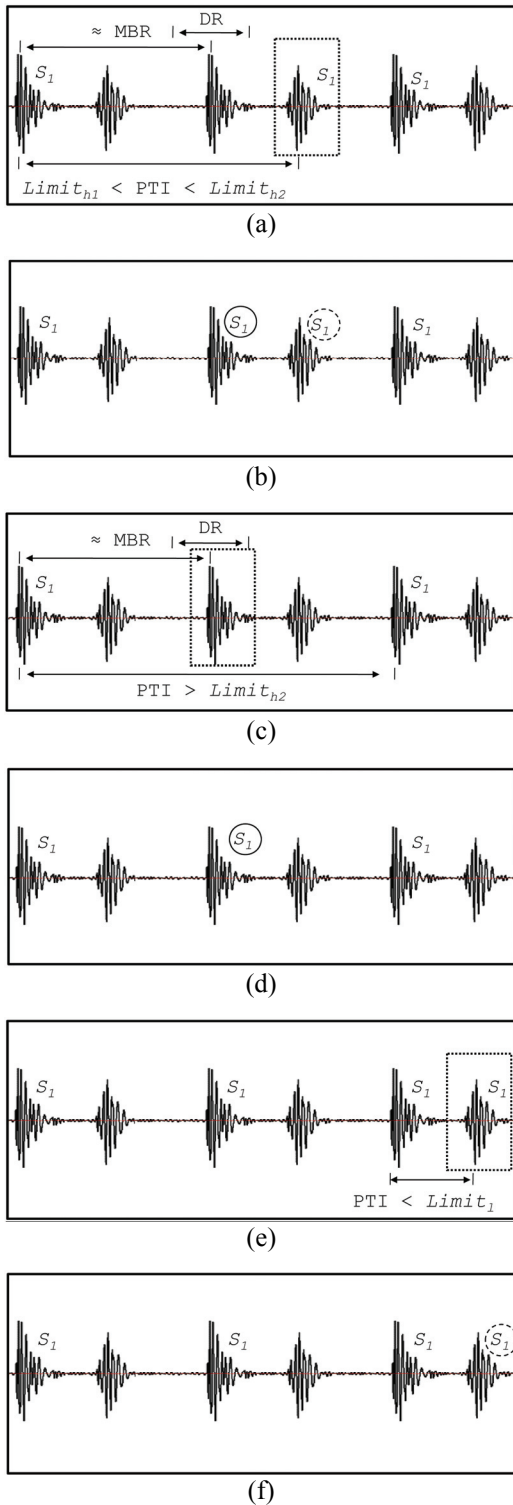


Fig. 5. S_1 detection problems and results of the Replace, Add, and Delete (RAD) algorithm. A solid circle indicates a newly added S_1 and a dotted circle indicates a deleted S_1 : (a) False detection of S_1 ; (b) The correction result by the ‘Replace’ procedure of (a); (c) Detection failure of S_1 ; (d) The corrected result by the ‘Add’ procedure of (c); (e) Duplicated S_1 detection; (f) The result of the ‘Delete’ procedure of (e).

In Fig. 5, dotted box shows the detection problem with S_1 detection. Fig. 5(a) indicates a false detection of S_1 when PTI is between $Limit_{h1}$ and $Limit_{h2}$. Fig. 5(b) shows the corrected result of the ‘replace’ procedure for (a). A new S_1 is detected with the mean beat rate (MBR) and detection range (DR). MBR is decided with the average value of the previous S_1 time difference and DR is 0.2 s, empirically. The second detection problem is shown in Fig. 5(c). A S_1 is missed when PTI is longer than $Limit_{h2}$. Fig. 5(d) is the result of the ‘add’ procedure. In add procedure, S_1 is added by the same rule of replace method. However, in add procedure, the next S_1 would not be deleted because a S_1 is missed. The last detection problem is represented in Fig. 5(e). S_1 is detected again when PTI is shorter than $Limit_l$. Fig. 5(f) shows the result of the ‘delete’ procedure. In this procedure, the latter S_1 is deleted between two adjacent S_1 , and the former S_1 is retained.

Fig. 6 shows a flowchart of the RAD algorithm and S_2

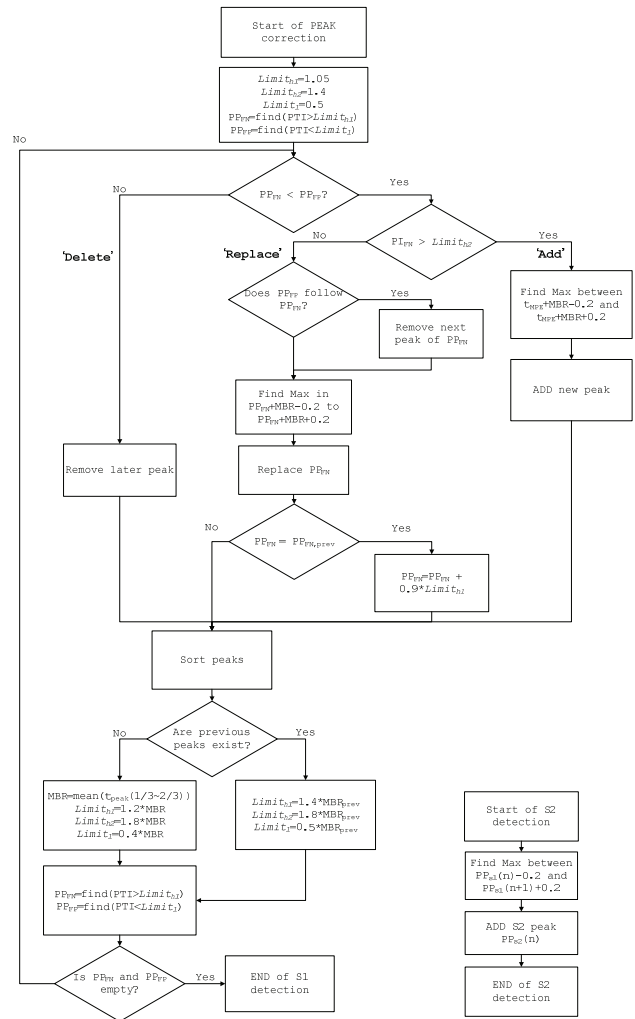


Fig. 6. Flowchart of the RAD algorithm and S_2 detection: (a) RAD algorithm for S_1 correction; (b) S_2 localization procedure. MBR = mean beat rate, PI = peak interval, $PP_n = n$ -th peak position.

detection. The RAD algorithm is repeated until every S_1 is corrected. The S_2 localization depends on S_1 detection and it is represented in Fig. 5(b). S_2 is determined by the maximum value position between two adjacent S_1 .

4. Evaluation

For localization performance evaluation, the true positive (TP), false positive (FP), false negative (FN) and failed detection (FD) were calculated. Then, we derived the sensitivity (SE), positive predictivity (+P), and failed detection rate (FDR) to evaluate the accuracy of the detection algorithm. Detected peaks were verified with a 200-ms approval range from the reference peak positions that were obtained by ECG-gated detection. Sensitivity was calculated using (13), +P using (14), and FDR using (15). Evaluations were carried out for both S_1 and S_2 localizations.

$$\text{Sensitivity (SE)} = \frac{\text{True Positive}}{\text{True Positive} + \text{False Negative}} \times 100 (\%) \quad (13)$$

$$\text{Positive predictivity (+P)} = \frac{\text{True Positive}}{\text{True Positive} + \text{False Positive}} \times 100 (\%) \quad (14)$$

$$\text{Failed detection rate (FDR)} = \frac{\text{Failed Detection}}{\text{Total Peaks}} \times 100 (\%) \quad (15)$$

5. Results

5.1 Signal conditioning

The signal conditioning results are shown in Fig. 7. Fig. 7(a) represents the original heart sound waveform, and (b), (c), and (d) are the CIC-filtered signal, Hilbert-transformed signal, and moving-average-filtered signal, respectively. In Fig. 7(d), the detected S_1 and S_2 peaks are described.

5.2 Peak correction and classification

The initially detected peaks after signal conditioning are processed with the FPPC and FNPC methods. The FPPC and FNPC results are represented in Fig. 8. Initially detected peaks are shown in Fig. 8(a), and Fig. 8(b) shows the PTI of (a). FPP and FNP could be detected with detection criteria (1) and (2), respectively, described as relatively low and high PTI values in Fig. 8(b). The corrected peak and its PTI are presented in Figs. 8(c) and 8(d), respectively. After peak correction, the S_1 and S_2 locations are decided at the up-or-down peaks of the PTI curve.

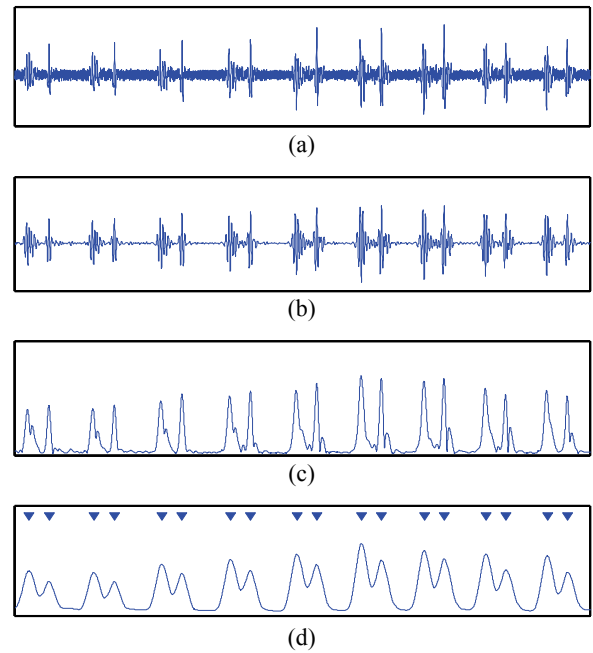


Fig. 7. Signal conditioning procedure and digital filtering: (a) Original heart sound; (b) CIC-filtered result ($M = 2$, $N_{\text{lpr}} = 16$, $N_{\text{hpr}} = 32$); (c) Hilbert-transformation result; (d) Moving average integrator result (window size=0.15 s). ‘▼’ indicates a detected peak.

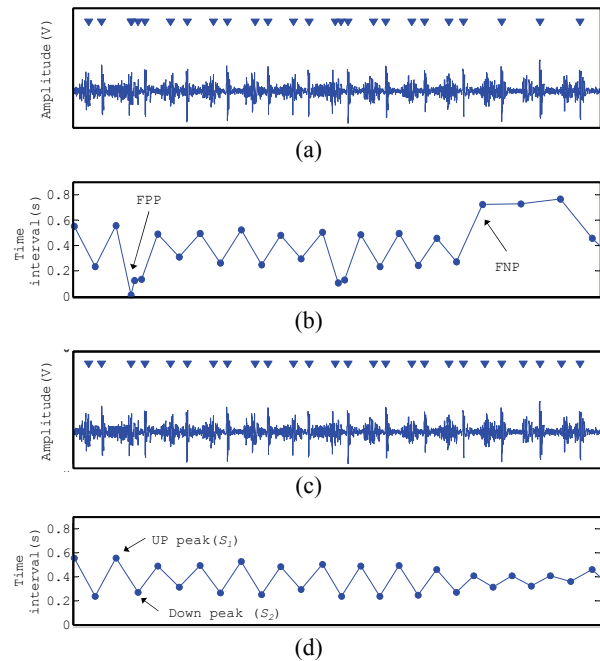


Fig. 8. Correction and classification of the detected peaks after signal conditioning: (a) Detected peaks by differential method; (b) Peak time intervals of (a). False positive peaks (FPP) and false negative peaks (FNP) were detected in this stage; (c) Corrected peaks. (d) Peak time intervals of (c). A longer time interval (UP peak) means a S_1 and shorter time interval (Down peak) means a S_2 peak.

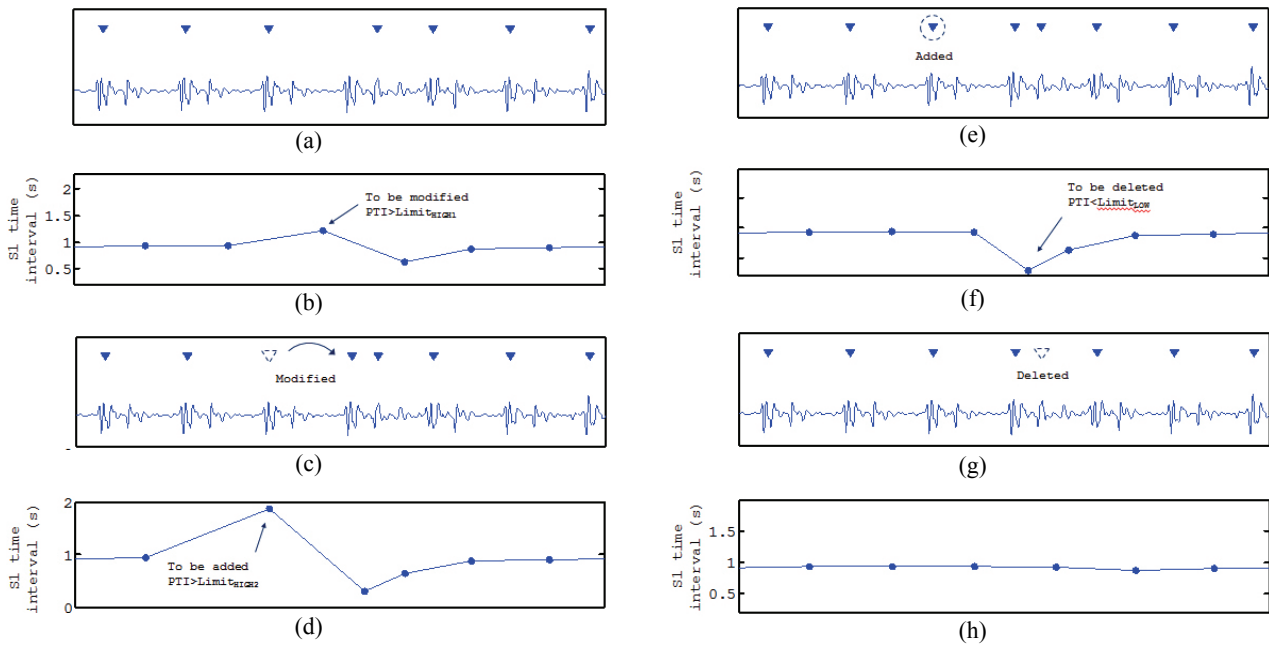


Fig. 9. An example of the S_1 correction method: (a) S_1 detection result before RAD algorithm. There is a misdetect peak between the 3rd and 5th peaks; (b) Peak time interval (PTI) of (a). It was found to be a $PTI > Limit_{HIGH1}$ peak; (c) ‘Replace’ procedure; (d) PTI of (c); (e) ‘Add’ procedure; (f) PTI of (e); (g) ‘Delete’ procedure; (h) PTI of (g).

Table 2. Results evaluating the S_1 detection algorithm at each stage. The method consists of CIC filtering, peak correction (PC), and the replace, add, and delete (RAD) algorithm

No.	Method	RS ₁ ^a (beats)	DS ₁ ^b (beats)	TP (beats)	FP (beats)	FN (beats)	FD (beats)	SE (%)	+P (%)	FDR (%)
1	Hilbert+MAF	27082	23783	23716	67	3366	3433	87.57	99.72	14.48
2	1+CIC filter	27082	25409	25397	12	1685	1697	93.78	99.95	6.68
3	2+PC	27082	25647	25643	4	1439	1443	97.69	99.98	5.63
4	3+RAD	27082	26358	26343	15	739	754	97.27	99.94	2.86

^aTotal number of reference S_1

^bTotal number of detected peaks

Table 3. Results evaluating the S_2 detection algorithm at each stage. The method consists of CIC filtering, peak correction (PC), and the replace, add, and delete (RAD) algorithm

No.	Method	RS ₂ ^a (beats)	RS ₂ ^b (beats)	TP (beats)	FP (beats)	FN (beats)	FD (beats)	SE (%)	+P (%)	FDR (%)
1	Hilbert+MAF	27082	22780	22780	0	4358	4358	83.94	100	19.13
2	1+CIC filter	27082	24394	24394	0	2697	2697	90.04	100	11.06
3	2+PC	27082	24824	24824	0	2264	2264	91.64	100	9.12
4	3+RAD	27082	25740	25740	0	1357	1357	94.99	100	5.27

^aTotal number of reference S_2 .

^bTotal number of detected peaks.

5.3 Replace, Add, and delete correction

Classified S_1 peaks were also corrected with the RAD algorithm. Fig. 9 shows an example of S_1 correction with the RAD algorithm. Fig. 9(a) and (b) show the initially detected S_1 and its PTI. RAD correction was carried out using (8), (9), and (10). Figs. 9(c) and (d), Figs. 9(e) and (f), and Figs. 9(g) and (h) show the replace, add, and delete procedures and the PTI, respectively.

5.4 Statistical evaluation

In the statistical analysis, SE, +P, and FDR were

calculated to evaluate the classification performance at each stage. The results of S_1 and S_2 localization are presented in Tables 2 and 3. In S_1 localization, SE was increased, 87.57% to 97.27%, and +P was increased, 99.72% to 99.94%. FDR decreased, 14.48% to 2.86%. Except for slight fluctuation in +P, each performance evaluation index was increased in every correction stage.

Performance for S_2 localization was evaluated in the same way as S_1 . In S_2 localization, SE increased, 83.94% to 94.99%, and +P was 100% in each case. FDR decreased, 19.13% to 5.27%. Each performance evaluation index of S_2 also increased in every correction stage. Overall localization performance for S_1 was better than for S_2

except in terms of +P.

6. Conclusion

6.1 Performance evaluation

The proposed method was validated by a quantitative study with 27,082 pulses, posture changes, and respiratory variation. Localization performance was most improved by CIC filtering; SE and FDR were improved by 6.21% and 7.8%, respectively, in the S_1 case. In the S_2 case, they were also improved, by 6.1% and 8.07%. +P was not changed significantly. Remaining misdetected peaks after frequency domain-filtering were corrected by peak correction and the RAD algorithm. These algorithms improved FDR by 1.05% and 1.95% in the S_1 case. These results could be considered as slight improvement; however, it is meaningful to recover from missing or extremely distorted peaks. Because S_2 detection depends largely on S_1 results, S_2 detection performance had a lower value than S_1 results; however, +P was always 100%.

6.2 Limitation

A time-dependent classification algorithm is hard to adapt to an irregular heartbeat. For example, the heart sound of an arrhythmia patient could generate more errors because a correction criterion is affected by the previous PTI and specific constant. An error could even be propagated in certain cases.

In S_2 localization, the S_2 detection rate depends on the S_1 detection result. Thus, failed detection of S_1 could be a reason of the failure of S_2 localization. The proposed algorithm focuses on a post-peak correction method of heart sounds; however, it does not provide a noise reduction method for the inherent problems of heart sounds. Major heart sound problems, such as lung sounds, murmurs, respiration effects, and signal distortion in female subjects, were not addressed significantly in this paper.

6.3 Concluding remarks

In this study, only heart sound data were used to localize S_1 and S_2 features, with no other reference signal. This is a novel study in heart sound localization because it may provide an efficient and accurate method for heart sound applications. From the research presented, it appears that the proposed first and second heart sound localization method can improve localization performance. It may be a useful method for robust peak detection in various applications, such as LVET/PEP detection and cardiac disorder diagnoses. Although there are still unsolved problem related to abnormal heart activity and optimization for robust detection, we believe that the proposed method can provide simple and reliable heart sound feature

detection.

Acknowledgements

This work was supported by the Soonchunhyang University Research Fund (No. 20120676)

This research was supported by the MSIP(Ministry of Science, ICT and Future Planning), Korea, under the C-ITRC(Convergence Information Technology Research Center) (IITP-2015-IITP-2015-H8601-15-1009) supervised by the IITP(Institute for Information & communications Technology Promotion)

References

- [1] RP Lewis, SE Rittogers, WF Froester, and H Boudoulas, A critical review of the systolic time intervals, *Circulation* 56 (1977) 146-58.
- [2] S Babaei and A Geranmayeh, Heart sound reproduction based on neural network classification of cardiac valve disorders using wavelet transforms of PCG signals, *Comput Biol Med* 39 (2009) 8-15.
- [3] A Bartels and D Harder, Non-invasive determination of systolic blood pressure by heart sound pattern analysis, *Clin Phys Physiol Meas* 13 (1992) 249-56.
- [4] XY Zhang, E MacPherson, and YT Zhang, Relations between the timing of the second heart sound and aortic blood pressure, *IEEE Trans Biomed Eng* 55 (2008) 1291-7.
- [5] SM Debbal and F Bereksi-Reguig, Automatic measure of the split in the second cardiac sound by using the wavelet transform technique, *Comput Biol Med* 37 (2007) 269-76.
- [6] SM Debbal and F Bereksi-Reguig, Computerized heart sounds analysis, *Comput Biol Med* 38 (2008) 263-80.
- [7] M El-Segaier, O Lilja, S Lukkarinen, L Sornmo, R Sepponen, and E Pesonen, Computer-based detection and analysis of heart sound and murmur, *Ann Biomed Eng* 33 (2005) 937-42.
- [8] C Gupta, R Palaniappan, S Swaminathan, and S Krishnan, Neural network classification of homomorphic segmented heart sounds, *Applied Soft Computing Journal* 7 (2007) 286-297.
- [9] P Hult, T Fjallbrant, K Hilden, U Dahlstrom, B Wranne, and P Ask, Detection of the third heart sound using a tailored wavelet approach: method verification, *Med Biol Eng Comput* 43 (2005) 212-7.
- [10] J Torry, Heart sound analysis comparing wavelet and autoregressive techniques, *Computers in Cardiology* (2003) 657-660.
- [11] I Turkoglu, A Arslan, and E Ilkay, An intelligent system for diagnosis of the heart valve diseases with wavelet packet neural networks, *Comput Biol Med*

- 33 (2003) 319-31.
- [12] A Voss, A Mix, and T Hubner, Diagnosing aortic valve stenosis by parameter extraction of heart sound signals, *Ann Biomed Eng* 33 (2005) 1167-74.
- [13] C Ahlstrom, A Johansson, F Uhlin, T Lanne, and P Ask, Noninvasive investigation of blood pressure changes using the pulse wave transit time: a novel approach in the monitoring of hemodialysis patients, *J Artif Organs* 8 (2005) 192-7.
- [14] A Johansson, C Ahlstrom, T Lanne, and P Ask, Pulse wave transit time for monitoring respiration rate, *Med Biol Eng Comput* 44 (2006) 471-8.
- [15] SJ Shah and AD Michaels, Hemodynamic correlates of the third heart sound and systolic time intervals, *Congest Heart Fail* 12 Suppl 1 (2006) 8-13.
- [16] A Iwata, N Ishii, N Suzumura, and K Ikegaya, Algorithm for detecting the first and the second heart sounds by spectral tracking, *Med Biol Eng Comput* 18 (1980) 19-26.
- [17] H Liang, S Lukkarinen, and I Hartimo, Heart sound segmentation algorithm based on heart sound envelopogram, *Computers in Cardiology* (1997) 105-108.
- [18] A. Moukadem, A. Dieterlen, N. Hueber, C. Brandt, Comparative study of heart sounds localization, *Proc. SPIE 8068, Bioelectronics, Biomedical, and Bio-inspired Systems V; and Nanotechnology V, 80680P* (2011) 99
- [19] H Liang, S Lukkarinen, and I Hartimo, A boundary modification method for heart sound segmentation algorithm, *Computers in Cardiology* (1998) 593-595.
- [20] T Oskiper and R Watrous, Detection of the first heart sound using a time-delay neural network, *Computers in Cardiology* (2002) 537-540.
- [21] A Yadollahi and Z Moussavi, A robust method for heart sounds localization using lung sounds entropy, *IEEE Transactions on Biomedical Engineering* 53 (2006) 497-502.
- [22] V Nigam and R Priemer, Accessing heart dynamics to estimate durations of heart sounds, *Physiol Meas* 26 (2005) 1005-1018.
- [23] A Ricke, R Povinelli, and M Johnson, Automatic Segmentation of Heart Sound Signals Using Hidden Markov Models, *Computers in Cardiology* 32 (2005) 953.
- [24] S Messer, J Agzarian, and D Abbott, Optimal wavelet denoising for phonocardiograms, *Microelectronics Journal* 32 (2001) 931-941.
- [25] P Wang, Y Kim, L Ling, and C Soh, First heart sound detection for phonocardiogram segmentation, *Conf Proc IEEE Eng Med Biol Soc* 5 (2005) 5519-22.
- [26] C Ahlstrom, T Lanne, P Ask, and A Johansson, A method for accurate localization of the first heart sound and possible applications, *Physiol Meas* 29 (2008) 417-28.
- [27] C Barabasa, M Jafari, A Robust Method for S_1/S_2 Heart Sounds Detection Without ECG Reference Based on Music Beat Tracking, *Electronics and Telecommunications (ISETC), 2012 10th International Symposium* (2012) 307-310.
- [28] G Amit, K Shukha, N Gavriely, and N Intrator, Respiratory modulation of heart sound morphology, *Am J Physiol Heart Circ Physiol* 296 (2009) H796-805.
- [29] A Haghghi-Mood and J Torry, A sub-band energy tracking algorithm for heart sound segmentation, *Computers in Cardiology* (1995) 501-504.
- [30] T Kohama, S Nakamura, and H Hoshino, An efficient RR interval detection for ECG monitoring system, *IEICE Transactions on Information and Systems E Series D* 82 (1999) 1425-1432.
- [31] H Baranek, H Lee, G Cloutier, and L Durand, Automatic detection of sounds and murmurs in patients with Ionescu-Shiley aortic bioprostheses, *Medical and Biological Engineering and Computing* 27 (1989) 449-455.



Se Dong Min He received the M.S. and Ph.D. degrees in electrical and electronic engineering from the Department of Electrical and Electronics Engineering, Yonsei University, Seoul, in 2004 and 2010, respectively. He is currently an Assistant Professor at the Department of Medical IT Engineering,

Soonchunhyang University, Asan, Korea. His research area includes biomedical signal processing, healthcare sensor application, and mobile healthcare technologies.



Hangsik Shin is the Assistant Professor at the Chonnam National University. He received the Ph.D. degree in electrical and electronic engineering from the department of Electrical and Electronics Engineering, Yonsei University, in 2010. His research area include biomedical signal processing,

physiological modeling, u-Healthcare and mobile Healthcare Technologies.